A Spring Propelled Extreme Environment Robot for Off-World Cave Exploration

Steven D. Morad
Space and Terrestrial Robotic Exploration (SpaceTREx) Laboratory
Dept. of Aerospace and Mechanical Eng.
University of Arizona
smorad@email.arizona.edu

Thomas Dailey
Space and Terrestrial Robotic Exploration (SpaceTREx) Laboratory
Dept. of Aerospace and Mechanical Eng.
University of Arizona
daileytommy@email.arizona.edu

Leonard Dean Vance
Space and Terrestrial Robotic Exploration (SpaceTREx) Laboratory
Dept. of Aerospace and Mechanical Eng.
University of Arizona
ldvance@email.arizona.edu

Jekan Thangavelautham
Space and Terrestrial Robotic Exploration (SpaceTREx) Laboratory
Dept. of Aerospace and Mechanical Eng.
University of Arizona
jekan@email.arizona.edu

***Abstract*—Pits on the Moon and Mars are intriguing geological formations that have yet to be explored. These geological formations can provide protection from harsh diurnal temperature variations, ionizing radiation, and meteorite impacts. Some have proposed that these underground formations are well-suited as human outposts. Some theorize that the Martian pits may harbor remnants of past life. Unfortunately, these geological formations have been off-limits to conventional wheeled rovers and lander systems due to their collapsed ceiling or "skylight" entrances. In this paper, a new low-cost method to explore these pits is presented using the Spring Propelled Extreme Environment Robot (SPEER). The SPEER consists of a launch system that flings disposable spherical microbots through skylights into the pits. The microbots are low-cost and composed of aluminium Al-6061 disposable spheres with an array of adapted COTS sensors and a solid rocket motor for soft landing. By moving most control authority to the launcher, the microbots become very simple, lightweight, and low-cost. We present a preliminary design of the microbots that can be built today using commercial components for under 500 USD. The microbots have a total mass of 1 kg, with more than 750 g available for a science instrument. In this paper, we present the design, dynamics and control, and operation of these microbots. This is followed by initial feasibility studies of the SPEER system by simulating exploration of a known Lunar pit in Mare Tranquillitatis.**

TABLE OF CONTENTS

1. INTRODUCTION

Pits on the Moon and Mars are geological mysteries that could provide valuable insight into past geo-history and serve as a shelter for human habitat (Fig. 1). Daga et al. discusses the reasoning for the exploration of these pits in a planetary science decadal survey report [1]. These pits are one of the most promising locations for future research outputs, because they shield inhabitants from solar radiation, micrometeorites, and temperature variations of hundreds of degrees [2], [3]. On the Moon and Mars, some of these pits are believed to remnants of lava tubes. On the Moon, some of these pits are in polar permanently shadowed regions and may contain water-ice. On Mars, they offer protection from UV light, provide nearly constant temperatures, and potentially nutrient-rich volcanic regolith. This makes lava tubes one of the likely candidates for past life on Mars [4]. These pits are relatively untouched by surface processes and are time capsules that can tell us about the early formation of the solar system.

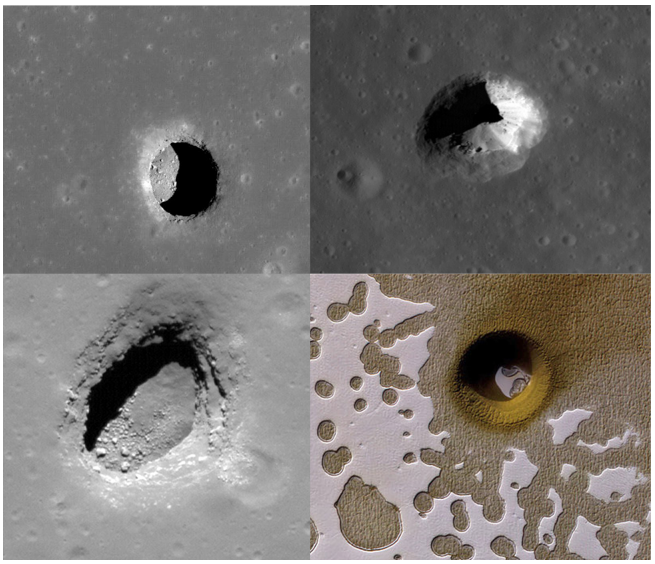

Figure 1: Lunar Reconnaissance Orbiter imagery of pits, (Top Left) Mare Tranquillitatis, (Top Right) Mare Fecunditatis (Bottom Left) Mare Ingenii. (Bottom Right) Example of a Martian pit taken by Mars Reconnaissance Orbiter [5].

Robots have not been sent inside an off-world pit, due to the difficulty and risk of vertically descending into a dark, unknown environment. To better understand if these pits harbor past-life or water, satellite observation is not sufficient [1]. Missions are required that provide in-situ measurements.

Entering these pits consists of surviving a vertical drop on the

978-1-5386-6854-2/19/$31.00 ©2019 IEEE

Symbol	Meaning
$\boldsymbol{Bold}$	Matrix
$\boldsymbol{bold}$	Vector
g	Lunar acceleration (1.625 m/s^2)
m	Bot mass (1 kg)
F	Force
J	Impulse
J_{net}	Net impulse
x	Launch spring displacement
t	Time
t_0	Time at launch
t_d	Time to move $d\boldsymbol{e}_x$
t_f	Time of terrain impact
v_0	Launch speed
v_f	Speed just before impact
v_i	Impact speed
θ	Launch angle
$E : \{\boldsymbol{e}_x, \boldsymbol{e}_y, \boldsymbol{e}_z\}$	Inertial frame
$B : \{\boldsymbol{b}_x, \boldsymbol{b}_y, \boldsymbol{b}_z\}$	Body-fixed bot frame
d	Horizontal distance to pit opening
h	Pit depth
$\boldsymbol{R}_0$	Rotation matrix from $\boldsymbol{e}_o$ to $\boldsymbol{e}_d$
$\boldsymbol{R}_1$	Rotation matrix from B to E
$\boldsymbol{e}_o$	Optimal impulse vector
$\boldsymbol{e}_t$	Tangent vector to $\boldsymbol{e}_d$
$\boldsymbol{e}_d$	Desired impulse vector
ϕ	Angle between $\boldsymbol{e}_o$ and $\boldsymbol{e}_d$
ϕ_e	Error in ϕ
w_0	Angular speed of wheel 0
w_1	Angular speed of wheel 1
w_s	Angular speed for spin stabilization
w_i	Angular speed for impulse modulation
w_f	Net angular speed
w_e	Error angular speed
w_a	Actual angular speed
$\boldsymbol{e}_f$	Unit vector for w_f
$\boldsymbol{e}_a$	Unit vector for w_a
$\boldsymbol{e}_e$	Unit vector for w_e
Δt_J	Impulse duration of thruster

Table 1: Notation used in this paper

order of one hundred meters [6]. The floor near the opening is covered with rubble, causing mobility challenges. The ceiling entrances may not be structurally sound, and may collapse as a heavy rover drives up to the edge. Most pit exploration platforms fall into one of two categories: a tethered rappelling robot such as AXEL [7], or microbots [8], including the SphereX platform [9] [10] [11] [12].

Whittaker discusses both microbot and tethered robot approaches in his Nasa Innovative Advanced Concepts (NIAC) proposal on the robotic exploration of these pits [13]. Tethered robots allow for a power and communications relay to be situated at the edge of the skylight, while a robot descends into the pit. JPL is currently pursuing this avenue with the AXEL and MoonDiver projects [7]. There are concerns that the tether may cause issues. First of all, Lunar regolith is extremely abrasive. So much so that during the Apollo missions, the regolith went into the astronauts' gloves [14]. It is possible that the motion of the tether on rock and regolith may cause accelerated damage to the tether. The tether from the surface robot to the descending robot rests on the edge of the skylight and is prone to collapse. Shifting rocks or a partial collapse while rappelling could cause the descending robot to swing into the wall, damaging or destroying the robot. Upon ascent a tethered robot could get lodged under a rock, causing a mission failure. That being said, tethers are a versatile approach that allow for extended time in the pits because of their ability to transfer solar energy from the surface. Many recent robotic platforms for Lunar pit exploration have started to converge towards the tethered design.

Microbots offset the risks of one expensive rappelling robot by allowing multiple microbots to fail, without sacrificing the mission [8]. Microbots would make their way to the opening of the pit, jump into the pit, and softly land using thrusters. Whittaker's concern with microbots is that they require extremely small components, that are decades away and may never actually exist. Designs like the SphereX microbot [9] [10] [11] [12] require fast reaction wheels and multiple microthrusters to land inside the pit. While these components now exists thanks to wide availability of CubeSat components, they are still more expensive than initially envisioned. For these reasons, we set out to design a simple and low-cost microbot for Lunar and Martian pit exploration. Our intention is to have platforms of various costs to be tailored to specific missions.

2. DESIGN

We propose the Spring Propelled Extreme Environment Robot (SPEER) system to develop a truly low-cost and disposable microbot. The SPEER system is a package consisting of a spring powered launcher and multiple microbot projectiles. The launcher uses a jack-in-the-box spring system to deploy one microbot at a time. Control happens before the bot leaves the launcher. A ballistic trajectory is computed and the bot is spin-stabilized by two wheels in the launcher before launch.

The microbot projectile is a AL-6061 (aluminium) sphere, 4 cm in radius with a solid-rocket motor, IMU, batteries, camera, and LTE radio (Fig. 2, Table 2). Other options were considered for propulsion including use of water-electrolysis propulsion [15] and water steam propulsion [16]. Both provide additional advantages including increased control authority, however the water waste product makes it inappro-

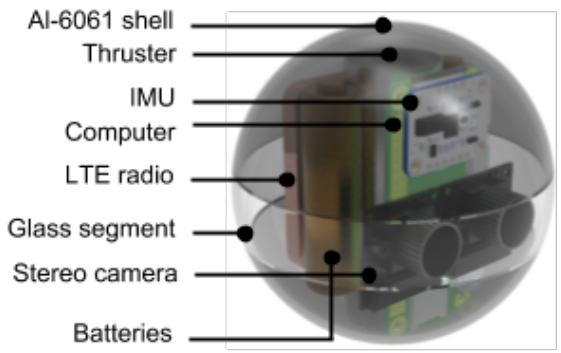

Figure 2: Rendering of the SPEER bot

Component	**Mass** (g)
2mm thick Al-6061 shell	102
2mm thick borosilicate glass	19
Estes D12-3 20N-s solid rocket engine	42
2×Energizer L91VP 4.5 Wh lithium battery	29
Raspberry-pi zero computer	9
2×Pi camera module	6
Adafruit 6-axis IMU	3
Sixfab 4G LTE radio	18
Wiring	3
Systems subtotal	**231**
Science payload	769
Total	**1000**

Table 2: Mass breakdown for a SPEER bot

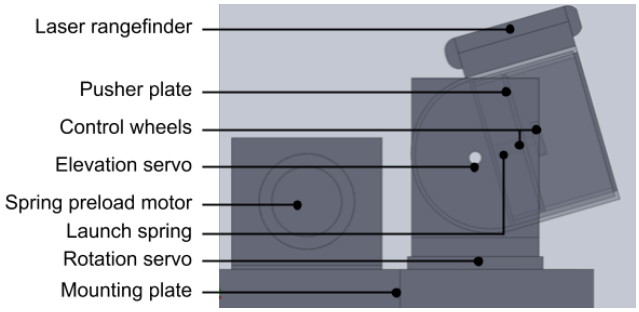

Figure 3: SPEER launcher diagram

Component	**Mass** (g)
$8 \times 8 \times 0.1$ cm aluminum pusher plate	17
Steel frame for pusher plate	20
PC105 4012 N/m spring	5
STP-MTRH stepper motor	3800
2×Pololu 1501MG high torque servo	120
2× Parallax 120RPM continuous servo	84
1m of 0.25 inch steel cable	160
2×JSumo 13.25mm radius silicone wheel	26
Margin for mounting plates and brackets	300
Raspberry-pi zero computer	9
Lightware SF11 laser rangefinder	35
Pi camera module	6
Total	**4592**

Table 3: Mass breakdown for a SPEER launcher

priate for science mission where the focus is to find water ice in the pits.

The electronics are rated to survive the estimated -20 ^{o}C environment of a Lunar pit [17]. Note that there is no reaction control system, which drastically cuts down on the mass of each microbot. The bot has room for science instruments, but other than that, it is a very simple system. By shifting all control to the launcher, large mass margins are afforded for science instruments and secondary payloads inside the bot.

A rover would drive a safe distance from the edge of a pit and launch a SPEER bot. As the bot flies into the cave, it collects valuable terrain data by fusing its stereo camera and IMU measurements. The bot then uses its solid-thruster to safely land. Stereo imagery and video is streamed in real-time to the rover, in case landing fails. This ensures even if the bot is destroyed on impact, valuable imagery of the pit is broadcasted on time. After landing, the microbot can unpack and utilize the onboard science instrument and transmit findings back to Earth via the rover (Fig. 5).

Spin Stabilization

The Lunar pits are on the order of one hundred meters deep, so a free-falling bot will impact at around 18 m/s. This is too fast to survive, so a powered descent is required. The bot will need to orient its thruster to soft-land. In spacecraft orientation this is usually done using a control moment gyro or with three separate reaction wheels. CubeSat-grade gyros and reaction wheels are heavy, slow and expensive.

Reaction wheels and gyros were not always available. Explorer-1 was the first satellite launched by the United States back in the 1950's but reaction wheels were not in use until the 1960's [18]. Explorer-1 utilized a method known as spin stabilization to orient itself. Spin stabilization is where a satellite spins along an axis to keep it pointed in a certain direction. The gyroscopic effect keeps the craft pointed toward its target, even with disturbances. We use spin stabilization to keep the SPEER oriented correctly.

The SPEER launcher has a camera and laser rangefinder to find a landing site for the bot. Given the range and elevation of the landing site, we can compute the bot trajectory before launch (Eq. 5). We find $\boldsymbol{v}(t_f)$, the velocity vector at the moment before impact (Eq. 11). A spin imparted along $\boldsymbol{v}(t_f)$ right before launch ensures the thruster stays pointed in the correct direction for a soft landing (Fig. 6, Eq. 16). This removes the need for any reaction control system in the microbot itself.

Soft Landing with a Solid-Fuel Engine

Efficient soft landing is difficult. Electric CubeSat thrusters do not provide enough force to counteract gravity on the Moon or Mars. Liquid-fuelled CubeSat engines have a mass

Component	Energy (mWh)
2×LV91VP Lithium battery	9000
Raspberry-pi zero computer	120
2×Pi camera module	200
Sixfab 4G LTE Radio	1100
Science Payload	variable

Table 4: Power budget for a SPEER bot. Only components using a significant amount of energy are shown.

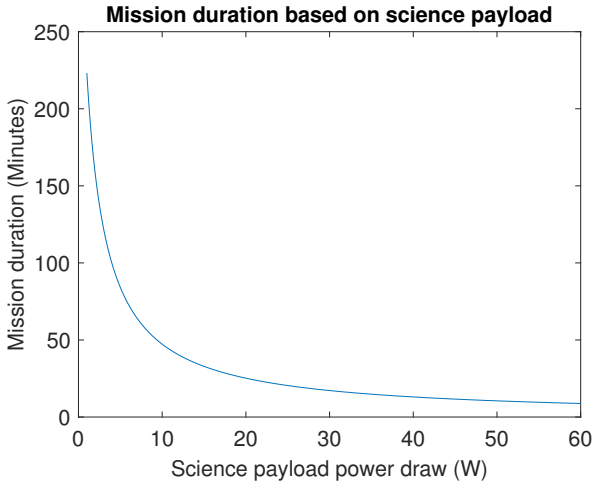

Figure 4: Mission duration based on the power draw of the science payload before losses.

of over one kilogram, partially due to the heavy pressurized fuel container and flow control system. Some liquid-fuel engines also require additional power to heat or cool the propellant before use. Solid-fuel engines used in model rockets do not have these requirements and are therefore very simple and light. They consist of a propellant and oxidizer packaged in a tube that is ignited by running current through a resistor.

The issue with using a solid-fuel engine is that they have a set impulse that cannot be changed. The engine cannot be easily shutdown and we do not know exactly how much Δv the SPEER bot will need before inspecting the cave. This would normally make solid-fuel engines unsuitable for soft-landing application, but in our case the thruster can be modulated by adding a torque-free precession to the bot using the launcher. The launcher uses powered wheels to create a precession by imparting a secondary angular velocity w_0, orthogonal to $\boldsymbol{v}(t_f)$. This allows us to reduce the net impulse by pointing the thruster away from $\boldsymbol{v}(t_f)$ (Fig. 7, Eq. 21).

3. Ballistics Analysis

We derive the equations of motion for the bot. Since the majority of the bot's flight is unpowered, it's motion is mostly ballistic with a soft-landing impulse J_{net}. The trajectory of the bot is illustrated in Fig. 8.

The bot leaves the launcher at time t_0 with launch velocity v_0 at angle θ. The compression of the launch spring x is computed as a function of v_0 using the following well

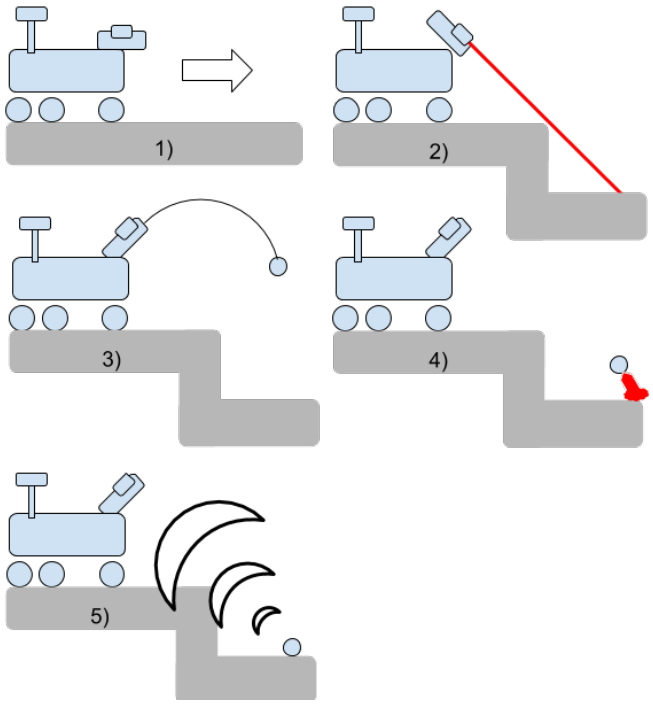

Figure 5: SPEER concept of Operations: 1) Drive to target. 2) Select landing site and find elevation using laser rangefinder, then compute trajectory. 3) Preload spring, apply spin, and launch. 4) Engine ignition and soft touchdown. 5) Utilize science instrument and relay data back to rover using radio.

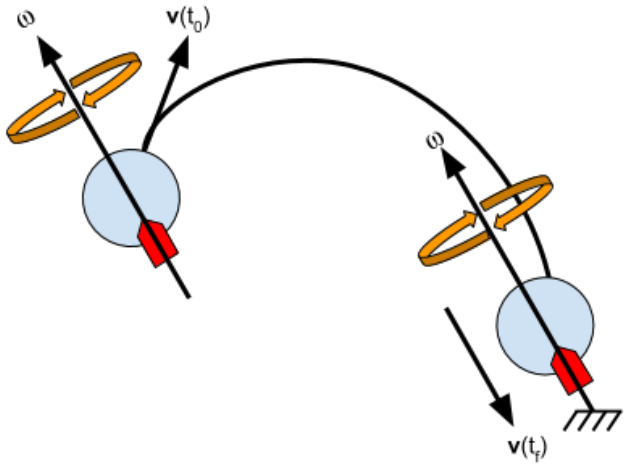

Figure 6: Spin stabilization of the SPEER. Angular velocity $\omega_f \boldsymbol{e}_o$ is imparted at t_0 (launch) to ensure the thruster stays pointed towards $\boldsymbol{v}(t_f)$.

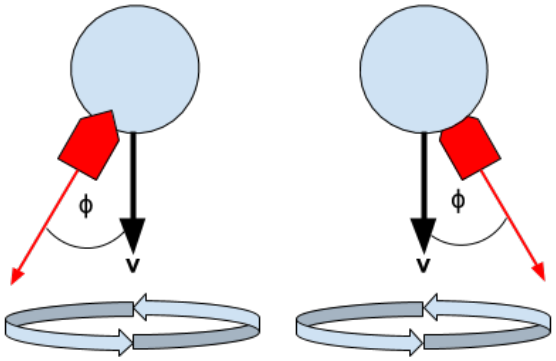

Figure 7: Adding precession allows modulating the net impulse of a solid-fuel rocket engine. Assume the bot is falling with velocity $\boldsymbol{v}$ along $-\boldsymbol{e}_z$. The thruster fires to soft-land. The precession causes the thruster to move in a circle about v. In the first instant, the thruster points at π. In the second instant, the thruster points at 2π. The thrust components in the plane orthogonal to v cancel, reducing the net impulse. By varying angle ϕ the net impulse J_{net} can be reduced to the desired impulse.

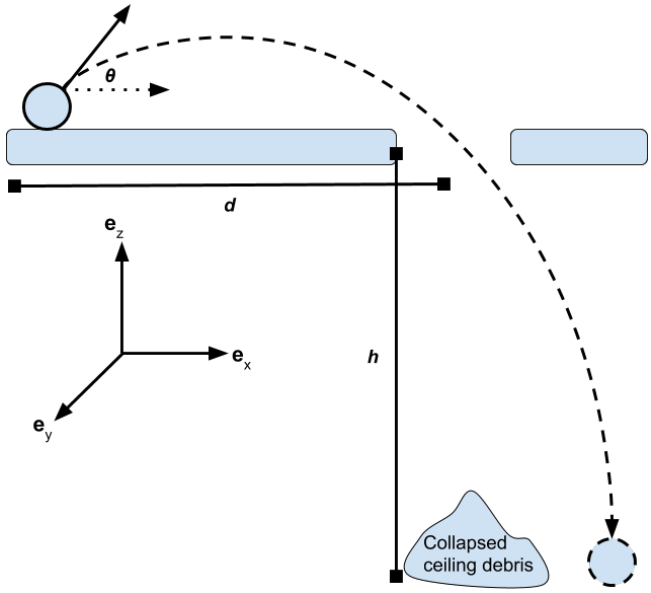

Figure 8: Visualization of SPEER ballistics

established equation:

$$x = v_0\sqrt{\frac{m}{k}} \tag{1}$$

The entire trajectory is in one plane so we can use planar dynamics. The acting forces are just gravity and an impulsive thrust.

$$\boldsymbol{F} = -mg\boldsymbol{e}_z + \boldsymbol{f}_T\delta(t_f - t) \tag{2}$$

$$\boldsymbol{a}(t) = -g\boldsymbol{e}_z + \frac{\boldsymbol{f}_T\delta(t_f - t)}{m} \tag{3}$$

Integrating we find

$$\boldsymbol{v}(t) = (-gt + v_0\sin\theta)\,\boldsymbol{e}_z + v_0\cos\theta\boldsymbol{e}_x + \frac{\boldsymbol{J}_{net}(t)}{m} \tag{4}$$

$$\boldsymbol{r}(t) = \left(\frac{-gt^2}{2} + v_0 t\sin\theta\right)\boldsymbol{e}_z + v_0 t\cos\theta\boldsymbol{e}_x + \int\frac{\boldsymbol{J}_{net}(t)}{m}dt \tag{5}$$

The impulse is instantaneous at t_f, so it can be ignored for most trajectory calculations. We compute the required launch velocity v_0 from the time to move $d\boldsymbol{e}_x$, t_d

$$\boldsymbol{r}(t_d)\cdot\boldsymbol{e}_z = 0 = t_d v_0\sin\theta - g\frac{t^2}{2} \tag{6}$$

$$t_d = \frac{2v_0\sin\theta}{g} \tag{7}$$

$$\boldsymbol{r}(t_d)\cdot\boldsymbol{e}_x = d = v_0\cos\theta t_d \implies d = v_0\cos\theta\frac{2v_0\sin\theta}{g} \tag{8}$$

$$v_0 = \sqrt{\frac{dg}{2\sin\theta\cos\theta}} \tag{9}$$

We can compute the velocity right before the instantaneous impulse, $v_f = ||\boldsymbol{v}(t_f)||$

$$\boldsymbol{r}(t_f)\cdot\boldsymbol{e}_z = -h = v_0\sin\theta t_f - g\frac{t_f^2}{2} \tag{10}$$

$$t_f = \frac{1}{g}\left(\sqrt{2gh + v_0^2\sin^2\theta} + v_0\sin\theta\right) \tag{11}$$

Plugging t_f into Eq. 4

$$\boldsymbol{v}(t_f) = v_0\cos\theta\boldsymbol{e}_x - \sqrt{2gh + v_0^2\sin^2\theta}\boldsymbol{e}_z \tag{12}$$

$$v_f = ||\boldsymbol{v}(t_f)|| = \sqrt{v_0^2 + 2gh} \tag{13}$$

4. Rotational Analysis

Now that the ballistics equations are derived, we analyze the rotation required for a soft landing. We must ensure the thruster is pointed correctly, resulting in the impulse J_{net} cancelling out the velocity such that $v(t_f) = 0$. The mass of the bot is distributed in such a way that the center of mass is in the center of the sphere. The thrust vector will always point through the center of mass, which means the thrust will not apply a moment or affect the rotation.

We define the negative of our optimal impulse vector in the inertial frame as

$$\boldsymbol{e}_o = \frac{\boldsymbol{v}(t_f)}{||\boldsymbol{v}(t_f)||} \tag{14}$$

and attach a body-fixed frame $B : \boldsymbol{b}_x, \boldsymbol{b}_y, \boldsymbol{b}_z$ to the bot such that the thruster points along the $-\boldsymbol{b}_z$ axis. Two wheels, $\{0, 1\}$ are used to orient the bot and apply angular velocities to the bot.

Applying Spin Stabilization

We want the bot to be robust against noise that would point the thruster ($-\boldsymbol{b}_z$) away from $\boldsymbol{e}_o$, so we spin stabilize about $\boldsymbol{e}_o$. We use $\boldsymbol{R}_0$ to align $-\boldsymbol{b}_z$ with $\boldsymbol{e}_o$

$$\boldsymbol{R}_0 = \begin{bmatrix} \cos\theta & 0 & -\sin\theta \\ 0 & 1 & 0 \\ \sin\theta & 0 & \cos\theta \end{bmatrix} \tag{15}$$

Now that $\boldsymbol{e}_o$ is aligned with $-\boldsymbol{b}_z$ We can spin wheel 0 at w_0 to impart an angular velocity of $-w_s\boldsymbol{b}_z$ to the bot. Let r_w be the radius of the wheel and r_b be the radius of the bot. Assuming no-slip between the wheel and bot, we have

$$\boldsymbol{w}_0 = \frac{w_s\boldsymbol{b}_z r_b}{r_w} \tag{16}$$

Using Eq. 16, we show how to apply a spin stabilization of $w_s\boldsymbol{b}_z$ to keep the thruster pointing towards $\boldsymbol{e}_o$ (Fig. 10).

Applying a Precession

Because of the nature of solid-fuel thrusters, we want to be able to modulate our net impulse by creating a torque-free precession of angle ϕ about $\boldsymbol{e}_o$ (Fig. 7). J_{net} is our desired impulse while J is the impulse rating of the thruster.

$$J_{net} = J\cos\phi = f_T\delta(t_f - t)\cos\phi \tag{17}$$

$$\phi = \arccos\frac{J_{net}}{J} \tag{18}$$

With ϕ, we construct rotation matrix $\boldsymbol{R}_1$. We can use this to compute our desired impulse magnitude J_{net} and desired impulse vector $\boldsymbol{e}_d$

$$\boldsymbol{R}_1 = \begin{bmatrix} \cos\phi & 0 & -\sin\phi \\ 0 & 1 & 0 \\ \sin\phi & 0 & \cos\phi \end{bmatrix} \tag{19}$$

$$\boldsymbol{e}_d = \boldsymbol{R}_1\boldsymbol{e}_o \tag{20}$$

After wheel 0 has spin stabilized the bot, wheel 1 rotates at w_1 along $\boldsymbol{b}_y$ to create a precession w_i to modulate the thruster impulse.

$$\boldsymbol{w}_1 = \frac{-w_i\boldsymbol{b}_y r_b}{r_w} \tag{21}$$

Eq. 21 tells us how fast to spin wheel 1 to apply a precession.

Nulling the Horizontal Components

To ensure that the horizontal components of the velocity are nulled, we need to make sure that the thruster completes full rotations over the impulse duration. One can imagine a case where the entire impulse happens over one quarter of a rotation, which would produce a nonzero impulse in the $\boldsymbol{b}_x, \boldsymbol{b}_y$ plane. We will find an expression for the magnitude w_f, such that the impulse happens over a multiple of $2\pi n$.

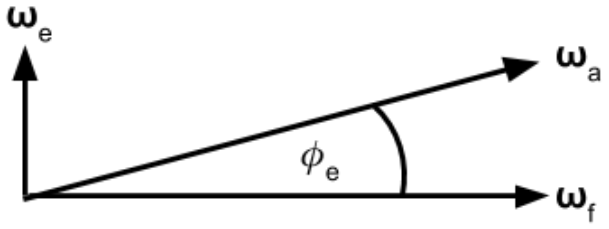

Figure 9: Geometric result of noise vector $\boldsymbol{w}_e$ on the actual axis of rotation $\boldsymbol{w}_a$

To complete n full rotations over a given impulse duration Δt_J we have

$$\frac{w_f}{\Delta t_J} = 2\pi n \tag{22}$$

So the angular velocity magnitude w_f is constrained by the impulse duration

$$w_f = 2\pi n\Delta t_J \tag{23}$$

A thruster that burns over one second would require w_f of $2\pi, 4\pi, 6\pi ...n$ rad/s.

The Effect of Noise on Impact Velocity

We generally want to pick the largest n we can. This reduces the divergence between the desired thruster direction $\boldsymbol{e}_d$ and the noise present in the actual thruster direction $\boldsymbol{e}_a$, ultimately reducing the impact velocity. We analyze how spin stabilization reduces the impact velocity v_i, to make for a softer landing. Let the actual spin $\boldsymbol{w}_a$ be a sum of the desired spin $\boldsymbol{w}_f$ and some error $\boldsymbol{w}_e$.

$$\boldsymbol{w}_a = w_f\boldsymbol{e}_d + w_e\boldsymbol{e}_t \tag{24}$$

We can express the $\boldsymbol{w}$ vectors geometrically with the resulting rotation vector w_a deviating from $\boldsymbol{e}_d$ by angle ϕ_e (Fig. 9).

We can find ϕ_e using the definition of the dot product

$$\phi_e = \arccos\left(\frac{\boldsymbol{w}_f \cdot \boldsymbol{w}_a}{||\boldsymbol{w}_f||||\boldsymbol{w}_a||}\right) \tag{25}$$

Thus, we can see how the optimal thruster direction $\boldsymbol{w}_f$ changes to $\boldsymbol{w}_a$ with noise $\boldsymbol{w}_e$.

We show exactly how this noise effects impact velocity v_i. Let $\boldsymbol{e}_f$, $\boldsymbol{e}_a$, and $\boldsymbol{e}_e$ be the unit vectors for the respective $\boldsymbol{w}$'s, with J_{net} being the instantaneous thruster impulse. Then we have

$$\boldsymbol{v}_i = v_f\boldsymbol{e}_f - J_{net}(\cos\phi_e\boldsymbol{e}_f + \sin\phi_e\boldsymbol{e}_e) \tag{26}$$

We want zero landing velocity so $J_{net} = v_f$

$$\boldsymbol{v}_i = v_f(1 - \cos\phi_e)\boldsymbol{e}_f + v_f\sin\phi_e\boldsymbol{e}_e \tag{27}$$

We find the impact magnitude as

$$||\boldsymbol{v}_i|| = v_i = v_f\sqrt{(1 - \cos\phi_e)^2 + \sin^2\phi_e} \tag{28}$$

$$v_i = v_f\sqrt{1 - 2\cos\phi_e + \cos^2\phi_e + \sin^2\phi_e} \tag{29}$$

$$v_i = v_f\sqrt{2 - 2\cos\phi_e} \tag{30}$$

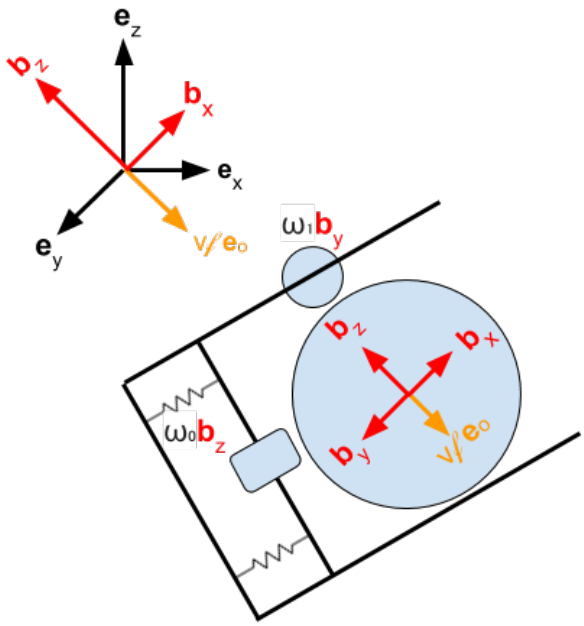

Figure 10: The wheels applying angular velocity to the bot. The body-fixed frame is in red, with the inertial frame in black. $\boldsymbol{b}_z$ is parallel to $\boldsymbol{e}_o$.

Putting it all Together

With spin stabilization component $\boldsymbol{w}_s$ and impulse modulation component $\boldsymbol{w}_i$, we can find an equation for the total angular velocity of the bot $\boldsymbol{w}_f$ (Fig. 10).

$$w_f \boldsymbol{e}_d = w_s \boldsymbol{b}_z + w_i \boldsymbol{b}_y \tag{31}$$

5. Discussion

One possible application of the SPEER robots is to probe lunar pits to determine if ice resides in them. As the temperature in the pits remains stable at around -20 ^{o}C, the conditions could be ideal for ice accumulation. To determine if there is ice in these pits, each SPEER would need to carry a science payload such as a compact neutron generator and detector. The other possibility is to just a carry a neutron generator and have the neutron detector on the rover. This would require line-of-sight between the rover and SPEER.

Science Payload

Large pieces of ice can be identified using the cameras, but that is not the case for smaller ice crystals dispersed in the regolith. NASA's curiosity rover carried an experiment called Dynamic Albedo of Neutrons (DAN). This experiment used a 14 MeV neutron generator to detect water and hydrated minerals up to 1m below the surface. Sandia National Labs recently designed a compact neutron generator, called the "neutristor". The neutristor was designed to be placed near tumors to allow cancer patients to continue their radiation therapy at home. As such, the neutristor was built to be powered by a single battery, with a compact 1.5 × 3cm form factor [19].

Like the DAN experiment, the neutristor also has an output energy of 14 MeV. Due to its low power usage and small size, it can easily fit inside a SPEER bot. In addition, the SPEER bot would ideally carry the neutron detector. Like the bots, the neutristor is disposable, with an operational time of 1000 seconds. Multiple bots can be launched to different places in the pit to find the areas with the highest concentration of ice or hydrated minerals.

Dynamics

Using the equations presented in the analysis, we can compute flight parameters for the pit discovered by Haruyama et al. Haruyama estimates the depth of the pit in the Mare Tranquillitatis as 80m [20]. We want to throw the bot in from distance $d\boldsymbol{e}_x$ so that the rover doesn't drive up to the unstable opening. We assume the bot is launched $d = 5$m from the cave opening, and that the depth of the cave is $h = 80$m (Fig. 8). Optimizing for maximum depth, the bot can soft-land after drops as large as 123.5m. For deeper pits, 14g of the science payload mass can be allocated for the larger 30 N-s thruster variant (Fig. 11a).

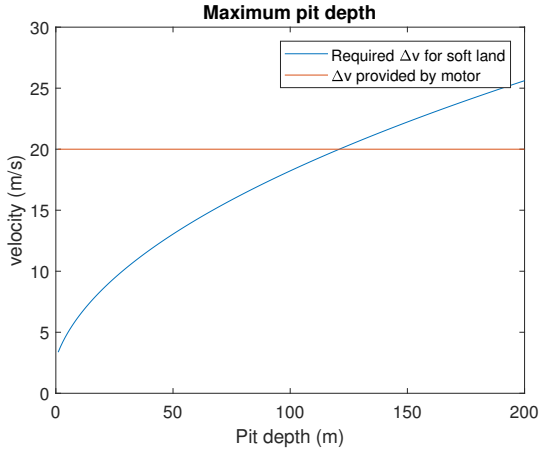

(a) The maximum depth of a pit is limited by the total impulse. This plot uses parameters: $d = 5$, $\theta = 45$ deg

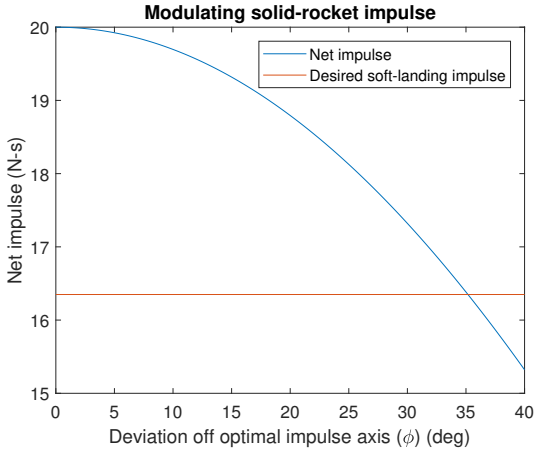

(b) Precession allows the throttling of a solid-fuel engine. For an 80m depth pit, 35 degrees of precession results in a soft-landing.

Figure 11: Soft landing requirements

We look at various launch angles θ. Since d is small, the difference in final velocities v_f is also small (Fig. 12a). This translates to a small change in the fuel required (Fig. 12b).

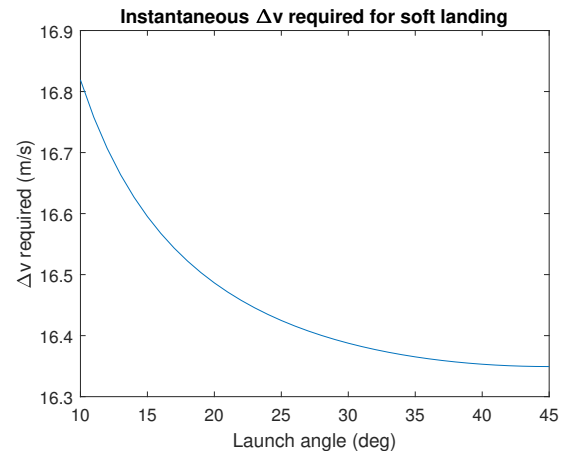

(a) Soft landing Δv requirements for various launch angles θ where $d = 5$m and $h = 80$m.

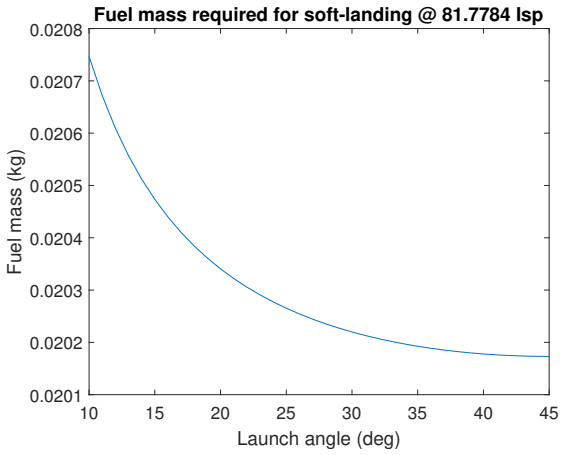

(b) Soft landing fuel requirements for various launch angles θ. The Estes D12-5 solid-fuel rocket engine contains 24.93g of fuel at 81.7784 I_{sp}.

Figure 12: Criteria used to select a value of θ

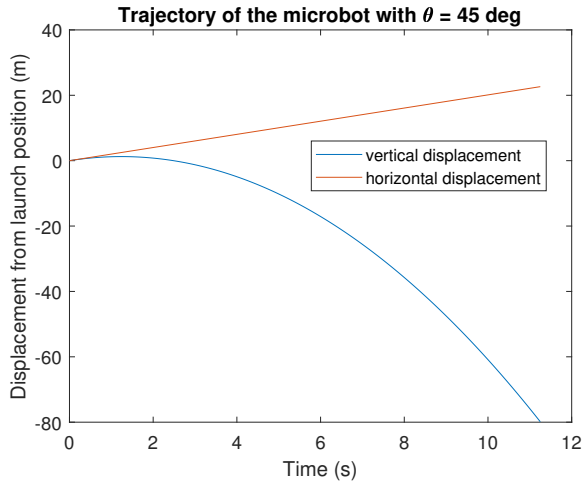

Figure 13: Ideal trajectory with $v_i = 0$ and how v_i varies with rotational noise

In a typical scenario, we select a launch angle of $45\,\mathrm{deg}$ and compute the trajectory of the bot using Eq. 5, plotted in Fig. 13. This results in a desired launch velocity $v_0 = 2.8460$ m/s. Using spring stiffness $k = 4012$ N/m, we use Eq. 1 to compress the spring $x = 4.49$cm to obtain our launch velocity.

6. Conclusion

We have proposed the SPEER system, which is made entirely of commercial components. The SPEER microbot costs under 500 USD each, with a total mass of 1 kg including up to 770 g of science payload. The components selected are capable of surviving the modest temperatures and low-radiation conditions of a Lunar or Martian pit. We have simulated a deployment of the SPEER architecture for exploration of a Lunar pit in the Marius hills and have provided numerical solutions for a soft touchdown. We have made some simplifying assumptions, but the values show that this is a feasible approach to off-world pit exploration.

SPEER better addresses the problem of microbot designs relying on small components that do not yet exist or are expensive. Certain components, like reaction wheels and liquid-fuel thrusters face reliability challenges due to miniaturization. We remove the need for the reaction wheels by externally spin stabilizing the bots. We add a second spin for impulse control, removing the need for a liquid-fuel thruster. This transfer of control authority from the microbot to the launcher allows for significant mass savings.

In-situ measurements provide a better picture of the inside of these pits than is possible with state-of-the-art recon satellites such as the Lunar Reconnaissance Orbiter (LRO). Lunar and Martian pits provide protection from radiation and diurnal temperature variations. On the Moon, they may contain water ice. On Mars, they may hold remnants of past life. Until we send robots inside them, we will not know. The SPEER system is a cost-effective, low-risk pathway for us to get a first look inside these off-world pits.

7. Future Work

The details of how the SPEER bots are packaged on the rover is not discussed. Some ideas are to place three of them to be packaged in an internally modified 3U PPOD, which would act like a magazine on a firearm.

We are working on building a SPEER prototype. We plan to experimentally test the performance of SPEER in the rugged environments of Arizona and New Mexico. If testing goes well, we plan to look into operating a SPEER system in a practical capacity on Earth. Mapping abandoned mine shafts too small for quadcopters or squeezing through tight crevasses to find trapped mountain climbers are just two Earth-based applications of the SPEER.

References

[1] A. W. Daga, C. Allen, M. Battler, J. Burke, I. Crawford, R. Léveillé, S. Simon, and L. Tan, "Lunar and martian lava tube exploration as part of an overall scientific survey," in *Annual Meeting of the Lunar Exploration Analysis Group*, vol. 1515, 2009, p. 15.

[2] J.-P. Williams, D. Paige, B. Greenhagen, and E. Sefton-Nash, "The global surface temperatures of the moon as measured by the diviner lunar radiometer experiment," *Icarus*, vol. 283, pp. 300–325, 2017, ISSN: 0019-1035.
[3] C. R. Coombs and B. Hawke, "A search for intact lava tubes on the moon: Possible lunar base habitats," 1992.
[4] R. J. Léveillé and S. Datta, "Lava tubes and basaltic caves as astrobiological targets on earth and mars: A review," *Planetary and Space Science*, vol. 58, no. 4, pp. 592–598, 2010.
[5] *New Views of Lunar Pits*. NASA, Sep. 2010.
[6] G. Cushing, T. Titus, J. Wynne, and P. Christensen, "Themis observes possible cave skylights on mars," *Geophysical Research Letters*, vol. 34, no. 17, 2007.
[7] L. Kerber, I. Nesnas, L. Keszthelyi, J. Head, B. Denevi, P. Hayne, K. Mitchell, J. Ashley, J. Whitten, A. Stickle, *et al.*, "Moon diver: A discovery mission concept for understanding the history of the mare basalts through the exploration of a lunar mare pit," in *New Views of the Moon 2-Asia*, vol. 2070, 2018.
[8] S. Dubowsky, K. Iagnemma, S. Liberatore, D. M. Lambeth, J. S. Plante, and P. J. Boston, "A concept mission: Microbots for large-scale planetary surface and subsurface exploration," *AIP Conference Proceedings*, vol. 746, no. 1, pp. 1449–1458, 2005.
[9] J. Thangavelautham, M. Robinson, A. Taits, T. McKinney, S. Amidan, and A. Polak, "Flying, hopping, pitbots for cave and lava tube exploration on the moon and mars," in *Proceedings of the 2nd International Workshop on Instrumentation for Planetary Missions*, 2014, pp. 1–4.
[10] L. Raura, A. Warren, and J. Thangavelautham, "Spherical planetary robot for rugged terrain traversal," in *Aerospace Conference, 2017 IEEE*, IEEE, 2017, pp. 1–10.
[11] H. Kalita, R. Nallapu, and J. Thangavelautham, "Guidance, navigation and control of the spherex robot for extreme environment exploration on mars," in *Proceedings of the 40th AAS Guidance and Control Conference*, 2017, pp. 1–12.
[12] S. Morad, H. Kalita, and J. Thangavelautham, "Planning and navigation of climbing robots in low-gravity environments," in *Position, Location and Navigation Symposium (PLANS), 2018 IEEE/ION*, IEEE, 2018, pp. 1302–1310.
[13] W. Whittaker, "Technologies enabling exploration of skylights, lava tubes and caves," *NASA, US, Report, no. NNX11AR42G*, 2012.
[14] L. Taylor, H. Schmitt, W. Carrier, and M. Nakagawa, "Lunar dust problem: From liability to asset," in *1st space exploration conference: continuing the voyage of discovery*, 2005, p. 2510.
[15] R. Pothamsetti and J. Thangavelautham, "Photovoltaic electrolysis propulsion system for interplanetary cubesats," in *IEEE Aerospace Conference, 2016*, IEEE, 2016, pp. 1–10.
[16] S. Rabade, N. Barba, L. Garvie, and J. Thangavelautham, "The case for solar thermal steam propulsion system for interplanetary travel: Enabling simplified isru utilizing neos and small bodies," in *Proceedings of the International Astronautic Congress, 2017*, IAC, 2017, pp. 1–9.
[17] D. Colter, "Down the lunar rabbit-hole," *NASA Science*, 2010.
[18] R. E. Roberson, "Two decades of spacecraft attitude control," *Journal of Guidance, Control, and Dynamics*, vol. 2, no. 1, pp. 3–8, 1979.
[19] J. M. Elizondo-Decanini, "Surface mounted neutron generators," in *APS Four Corners Section Meeting Abstracts*, 2012.
[20] J. Haruyama, K. Hioki, M. Shirao, T. Morota, H. Hiesinger, C. H. van der Bogert, H. Miyamoto, A. Iwasaki, Y. Yokota, M. Ohtake, *et al.*, "Possible lunar lava tube skylight observed by selene cameras," *Geophysical Research Letters*, vol. 36, no. 21, 2009.

BIOGRAPHY

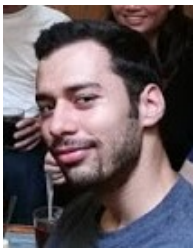

Steven D. Morad *is an aerospace engineering PhD student at the University of Arizona. He is currently a member of the Space and Terrestrial Robotic Exploration (SpaceTREx) Laboratory at the University of Arizona. Steven received his bachelor's in computer science at the University of California, Santa Cruz. He previously worked on operating systems and automation at Facebook. Steven is currently interested in autonomy for extreme off-world environments, such as Lunar pits and the surface of icy moons.*

Thomas Dailey *is an undergraduate student in systems and industrial engineering at the University of Arizona. He is an undergraduate researcher for the Space and Terrestrial Robotic Exploration (SpaceTREx) Lab. Thomas is interested in spacecraft design and shape memory alloys.*

Jekan Thangavelautham *has a background in aerospace engineering from the University of Toronto. He worked on Canadarm, Canadarm 2 and the DARPA Orbital Express missions at MDA Space Missions. Jekan obtained his Ph.D. in space robotics at the University of Toronto Institute for Aerospace Studies (UTIAS) and did his postdoctoral training at MIT's Field and Space Robotics Laboratory (FSRL). Jekan is an assistant professor and heads the Space and Terrestrial Robotic Exploration (SpaceTREx) Laboratory at the University of Arizona. He is the Engineering Principal Investigator on the AOSAT I CubeSat Centrifuge mission and is a Co-Investigator on SWIMSat, an Airforce CubeSat mission concept to monitor space threats.*